Journal of Sound and Vibration (2000) **230**(1), 69–99
doi.10.1006/jsvi.1999.2614, available online at http://www.idealibrary.com on IDEAL®

PRELIMINARY EXPERIMENTS ON NOISE REDUCTION IN CAVITIES USING ACTIVE IMPEDANCE CHANGES

O. LACOUR, M. A. GALLAND AND D. THENAIL†

Laboratoire de Mécanique des Fluides et d'Acoustique, UMR CNRS 5509,
Ecole Centrale de Lyon, B.P. 163, 69131 *Ecully Cedex, France*

(*Received* 20 *October* 1998, *and in final form* 1 *July* 1999)

This paper reports experiments on the active control of enclosed sound fields via wall impedance changes. Two methods previously developed allow one to implement practically active acoustic impedances: the first is referred to as "direct" control and permits precise realizations for harmonic excitations, while the second is a hybrid passive/active feedback control well suited for random noise treatments. The two techniques have been already presented [1]; the contribution of this work relies on testing the efficiency of both systems in silencing two enclosures through experimental analyses, subsequently compared with classical analytical description. The first test cavity is one-dimensional; a global sound reduction is achieved by the hybrid system for a broadband primary excitation. The second system is a reactangular three-dimensional cavity closed by a simply supported elastic plate. The noise source is an external load applied at one point of the plate. Different impedance values are successively assigned, their effect being estimated through a global sound level indicator. Attention is also given to plate vibration changes, which may occur. Three typical behaviours of the plate–cavity system are investigated. A first experiment involves an excitation at an acoustic resonance and induces a weak plate–cavity coupling. The second, also at an acoustic resonance of the cavity, yields a strong coupling while the third corresponds to an off-resonance excitation. The hybrid feedback control system provides useful attenuation for all cases, and shows also a promising behaviour when dealing with broadband excitations. It confirms the interest of the method when classical feedforward active control fails, i.e., when reliable prior information of the undesired disturbance is not available.

1. INTRODUCTION

The relevance of active techniques in controlling sound fields has long been the subject of important research, and many control strategies were built up for this purpose. The first one, suggested in 1936 by Lueg [2], consisted in superposing a secondary acoustic wave 180° out of phase with the unwanted sound. This technique has been generally termed active noise control (ANC), and impressively

†Current address: PSA Peugeot Citroen, DTAT/DMTC/MTS/MDN, Route de Gisy, 78140 Velizy Villacoublay, France.

0022-460X/00/060069 + 31 $35.00/0

developed thereafter, as described in the book by Nelson and Elliott [3]. More recently, a new and attractive approach, the active structural acoustic control (ASAC), has been proposed by Fuller and Jones [4]: structural loads are used as secondary sources to minimize the acoustic power radiated or transmitted through flexible walls. Application of these strategies often relies on a feedforward scheme and the availability of a reliable prior information of the unwanted noise. The latter assumption is not always acceptable: various problems which involve distributed random excitations, for instance, cannot be tackled through feedforward control so that an active solution with collocated sensors and actuators should be favoured. Within the prospect of active methods based on the concept of local feedback design, this paper studies the potentialities of a third strategy based on boundary condition control [1]: active systems are exploited in order to assign the most suited wall impedance for noise control. This strategy may be compared in its essence with other active methods attempting to provide additional damping to mechanical systems.

In this work, emphasis is given to the control of enclosed sound fields. Among the contributions preceding this paper, the uncoupled acoustic problem (no feedback action of the fluid towards flexible wall vibrations) has been first considered in an attempt to determine "the best that can be achieved" in terms of global sound attenuation in a cavity. Assuming the prior knowledge of the primary disturbance, different approaches for the control of one-dimensional fields were compared theoretically and experimented by Curtis *et al.* [5, 6]. They chose the total acoustic energy as cost function to be minimized and successively examined either suboptimal or optimal strategies. In particular, they established that a local pressure release at the end of a plane waveguide effectively suppresses the original resonances but introduces new ones. In the same context, an absorbing termination was also seen to produce large noise reductions at initial resonances and a weak increase at primarily low-level locations. Finally, it has been recognized that the ideal situation implies the total acoustic energy be minimized at any frequency: this allows defining the optimal strategy, which induces the greatest overall reduction. However, practical applications necessitate a microphone spatial sampling in order to provide the controller with a proper estimate of the acoustic energy. Moreover, the optimal transfer function between the primary and secondary sources leads to a non-causal behaviour and limits effective implementations to problems of quasi-periodic disturbances. Considering three-dimensional enclosed sound fields, works by Nelson and Elliott [3] faced again causality restrictions, which prevent the optimal action of secondary sources, in addition to other constraints such as controllability and observability (the adequate location of control sources and sensors). Clark and Cole [7] and Clark *et al.* [8] recently reformulated the problem in order to overcome the limitations that have been reviewed and to improve the active control of reverberant sound fields via feedback systems.

In fact, the pressure field in a cavity results in many cases from a complex process including vibroacoustic coupling effects through the walls. Intensive works have been devoted to the active control of noise radiated by structures. One of the first published contributions including an acoustic–structural coupled system was provided by Deffayet and Nelson [9] and devoted to the reduction of flexible

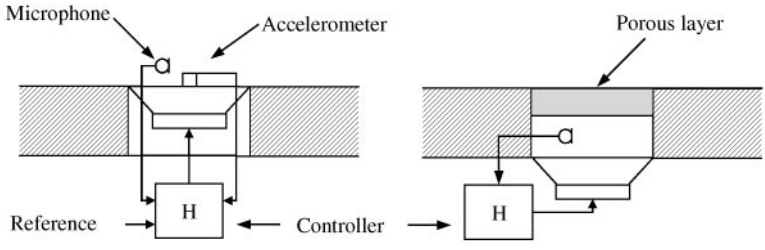

Figure 1. Impedance control methods.

panels radiation by active means. They attempted in their analytical study to reduce the acoustic radiation of a baffled rectangular plate by using secondary acoustic monopole sources, and demonstrated the requirement of the secondary source distribution to properly match the panel dominant mode. At the same time, a new approach appeared, involving vibratory sources fixed at the structure as control actuators; this method was named active structural acoustic control (ASAC) [4, 10, 11]. It came out that significant attenuation could be obtained with a relatively small number of control sources, at the expense of side-effects such as *modal restructuration* or *modal suppression*, not well foreseeable [12–15] and apparent only once the control was applied. Only a few decisive experiments were conducted without the accurate knowledge of the primary disturbance, as stated in the recent book by Fuller *et al.* [16].

Recently, there has been increasing interest in sound absorption by active or semi-active means and in impedance control, due to the limits that other active strategies reveal. Initial experiments were achieved by Guicking and co-workers [17–19], and followed by different techniques [1, 19–25], including contributions by the Laboratory of Fluid Mechanics and Acoustics at Ecole Centrale de Lyon [1, 21, 23]. The two methods used in order to obtain active absorbent surfaces are depicted in Figure 1 (see reference [1]). The first system (Figure 1, left) achieves the direct control of the acoustic impedance of a loudspeaker by a feedforward technique derived from the "filtered-X" LMS algorithm. Digital signals of pressure and velocity are combined in order to synthesize the error signal: $\varepsilon = p - Zv$, where Z is a real constant, the impedance to be achieved. The second method (Figure 1, right) was first suggested by Olson and May [26]: it is an efficient feedback method, say "hybrid", which combines a local active pressure reduction at one side of a porous layer, in conjunction with its low-frequency viscous properties, in order to drive the other side's impedance to the desired value. Clearly, its relatively low-cost design and its simplicity match much better the application of active means towards broadband unexpected excitations in realistic environments. Indeed, the control source is driven so as to produce a local pressure release "only", whereas more involved signal sensing and processing devices are required for the other methods reviewed. Experiments addressing the reliability of both systems for normal and oblique incidence are reported in reference [1].

In this paper, the efficiency of impedance control in reducing enclosed sound fields, for two vibroacoustic systems is examined experimentally. The study is restricted to low-frequency problems where both acoustic and structural fields

present a low modal density. The two reference cavities retained include an active impedance at a wall, and also allow classical analytical investigations to be simultaneously conducted. In the first part, the main conclusions obtained from a one-dimensional cavity excited at one single frequency are recalled [27]. Additional experiments involving broadband noise through hybrid control are also compared with analytical predictions. Next, a three-dimensional cavity is under investigation. An active impedance is positioned as part of the bottom wall of a rectangular cavity, while the upper wall is a simply supported elastic plate solicited by an external load. The modelling used exploits previous works by Dowell *et al.* [28], Pan *et al.* [29], and Hong and Kim [30]. It reveals that the plate and the cavity may be either weakly or strongly coupled, and agrees very well with experimental data. The work is partly focused on characteristic frequencies (on- or off-acoustic resonances) for which the effect of an impedance control is pointed out via the variations of acoustic and vibrational energies. Then, stating that most problems involving periodic excitations would allow the engineer to attempt feedforward control (i.e., to provide the controller with an accurate upstream reference of the disturbance), broadband excitations are analyzed to show the potentialities of feedback impedance control when the former method cannot be applied.

2. BROADBAND IMPEDANCE CONTROL IN A ONE-DIMENSIONAL CAVITY

2.1. DESCRIPTION AND ANALYSIS OF THE ONE-DIMENSIONAL CAVITY

Active noise control for reducing one-dimensional sound fields has been widely investigated. The approach in this paper is to use the acoustic impedance as control parameter, with a view to testing the active systems for broadband disturbance applications. Here a guide of length l represented in Figure 2 is considered where only plane waves propagate. A primary source, vibrating harmonically with a fixed amplitude value v_0 is at the left, while a controlled impedance Z_l is at the right. The acoustic energy in the cavity is the cost function to be minimized. The uncontrolled case corresponds to a perfectly rigid termination. The one-dimensional case allows simple analytical calculation [27]; the optimal impedance, which leads to a minimum energy in the guide, is

$$Z_{opt} = -\mathrm{j}Z_0 \tan kl, \tag{1}$$

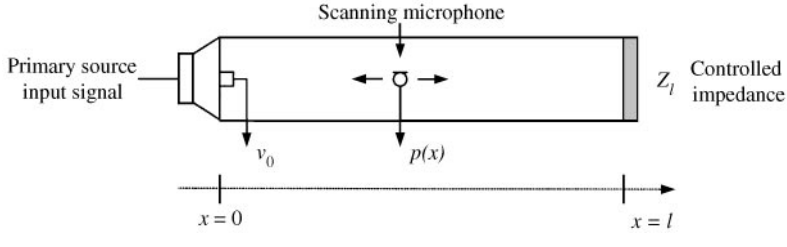

Figure 2. One-dimensional cavity.

where $k = \omega/c_0$ is the wave number, and $Z_0 = \rho_0 c_0$ is the air characteristic impedance. The minimum of the total acoustic energy becomes

$$E_t = \frac{\rho_0 v_0^2 l}{4}. \tag{2}$$

It may be checked that Z_{opt} at $x = l$ is the impedance which induces $Z(x) = 0$ at $x = 0$: the optimal impedance neither supplies nor absorbs any power while also preventing sound power radiation by the primary source.

In the important case of a rigid cavity resonance, where $k_n l = n\pi$, the optimal impedance becomes null. Thus, the best global sound reduction is achieved by a pressure release at the end of the guide. This result may also be interpreted in the following manner: assigning a terminal pressure release is equivalent to adding a "virtual" $\lambda/4$ length, in such a way that an initially resonant frequency exhibits an anti-resonant sound field. These results supported by preliminary experiments in reference [27] refer clearly to the work by Curtis *et al.* [5, 6], who stated the problem in a different way. The practical achievement of the optimal impedance is bounded by two limits, namely the frequency dependence and the non-causal behaviour relative to the primary source. As previously seen, the optimal impedance given by equation (1) implies a remote sound cancellation (at $x = 0$), an objective which cannot be handled by a feedback system for random excitations. In other words, attempting the practical achievement of equation (1) is an issue for periodic excitations only. Reducing noise generated by a random excitation favours a suboptimal strategy, based on sound absorption.

The corresponding set-up consists of a 0·88 m long tube terminated by a loudspeaker at $x = 0$ and by a controlled impedance at $x = l$ realized via the two techniques presented above. For broadband excitations, three different values of the terminal impedance have been experimented: the rigid termination case, the null impedance achieved with the direct method by using the signal feeding the primary source as controller reference input, and the absorbing termination achieved by the feedback hybrid method. Recall that it includes a porous layer whose low-frequency acoustic behaviour is mainly described by its flow resistivity σ such that

$$\sigma = \Delta P / V \Delta x,$$

where V is the flow crossing the porous layer of thickness Δx, induced by a static pressure drop ΔP. At asymptotically low frequencies, the same relation holds with acoustic quantities. Thus, if the acoustic pressure vanishes at the rear face of the absorbent, the layer input impedance becomes

$$Z = P/V = \sigma \Delta x.$$

It follows that a good low-frequency absorber results from a suitable material sample, when the flow resistance becomes $\sigma \Delta x = Z_0$, the air impedance [1, 26].

This value is practically reached by adjusting the sample thickness: a 1-cm-thick fibreglass sample in the experiments. Feedback control is achieved through an analogue filter for compensating the secondary-source response. A controller having two conjugate poles and zero pairs, a structure recognized by Carme [31] as the most appropriate for active control in a headset has been used. A classical pole-zero placement technique allows the controller both to provide a high noise reduction for low frequencies and to avoid instabilities of the closed-loop system. This set-up forms the electronic part of an almost anechoic device over the 100–500 Hz frequency range as shown by the absorption curve in Figure 3. The sound pressure level is scanned along the tube axis with a microphone. Like Curtis *et al.* [6], the index $J_p = \sum_{i=1}^{N_m} |p(x_i)|^2$ ($N_m = 44$ in the experiments) is used as an estimate of the potential acoustic energy which is representative of the total acoustic energy (except for very low frequencies under the first anti-resonance).

2.2. RESULTS AND COMMENTS

Figures 4 and 5 show the theoretical and experimental acoustic potential energy for some values of the reduced impedance given by $\zeta = Z/Z_0$ (the decibel values are not referenced). The initial behaviour of the rigid terminated one-dimensional cavity (thin solid line) corresponds to the ζ_∞ case. The theoretical and experimental results reported in the graphs reveal general trends in good agreement. The main discrepancy concerns the maximum values that can be observed (at resonances and anti-resonances of the rigid cavity) since no damping has been included in the analytical calculations. Figure 4 allows checking that the optimal impedance ensures the best reductions over the frequency range considered, and that in the vicinity of an initial resonance frequency, a reduction equivalent to that of the null impedance is obtained. It also comes out that the null impedance produces new resonances for frequencies where the original energy level was minimum. In

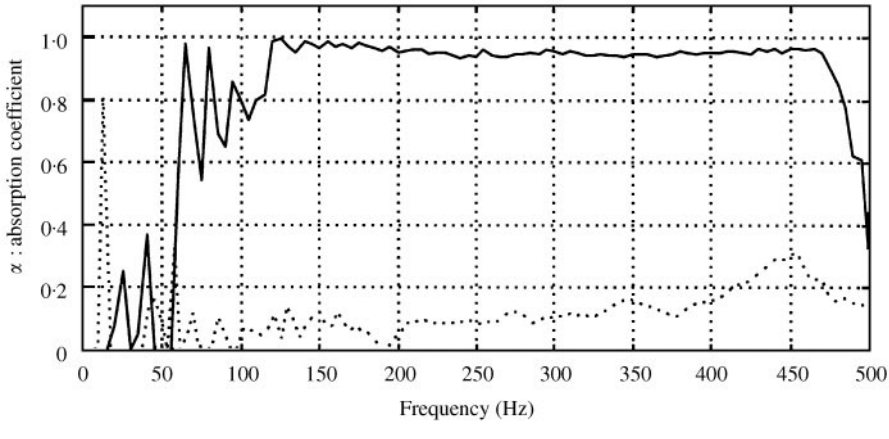

Figure 3. Absorption coefficient of the fibreglass sample versus frequency: ——, feedback control on; · · · · ·, porous material on a rigid plane.

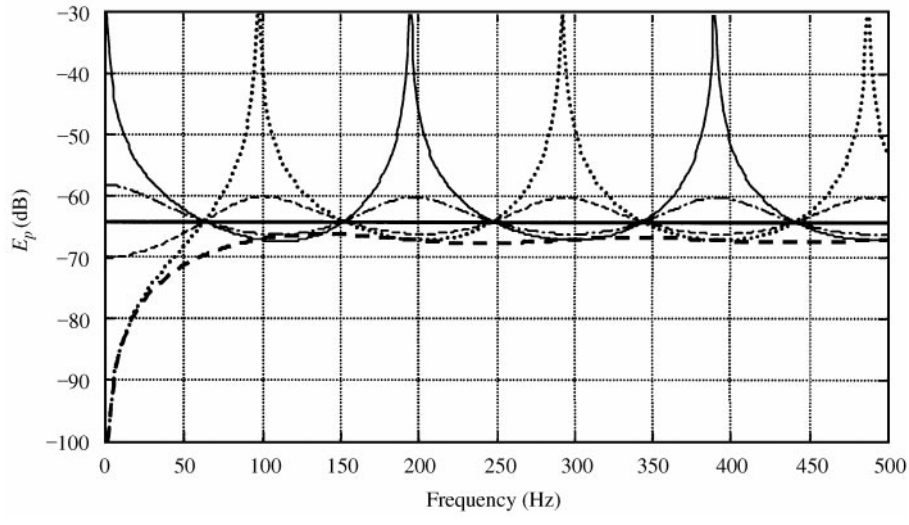

Figure 4. Theoretical acoustic potential energy evolution for different reduced impedances: · · · · · ·, $\zeta = 0$; – – –, $\zeta = 0{\cdot}5$; —, $\zeta = 1$; – · –, $\zeta = 2$; —, ζ_∞; – –, ζ_{opt}.

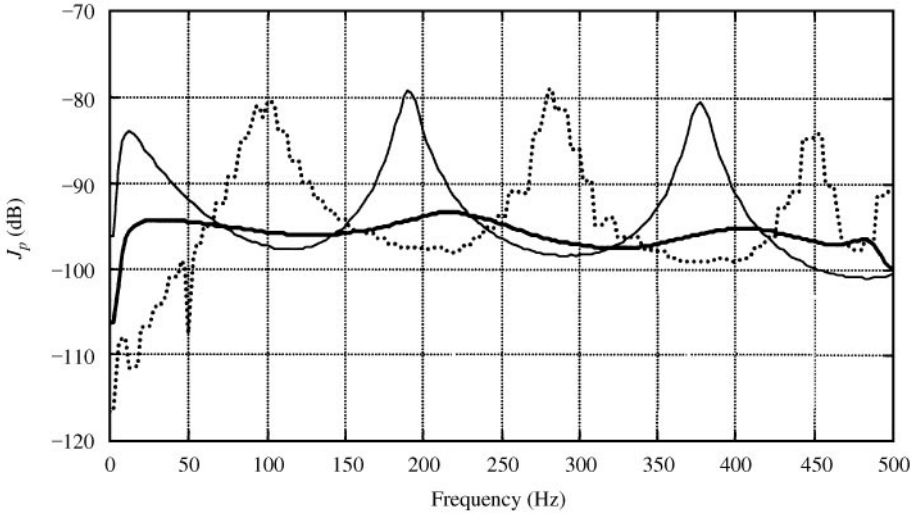

Figure 5. Experimental acoustic potential energy evolution for different reduced impedances: · · · · · ·, $\zeta = 0$ (LMS algorithm); —, $\zeta_{porous} \approx 1$ (feedback loop); —, ζ_∞.

comparison, the total absorbing termination ($\zeta = 1$) appears as an interesting compromise at all frequencies. It may be noted that similar remarks were drawn by Nelson *et al.* [32], who recognized an increasing interest in absorbing devices to silence systems when the causality constraint and the random nature of the disturbance add to the complexity of the problem.

3. IMPEDANCE CONTROL IN A 3-D STRUCTURAL–ACOUSTIC COUPLED SYSTEM

The set-up has been designed so that the following properties, allowing clear teachings, are verified: (1) the geometry is simple, (2) various coupling situations may be readily observed, and (3) for each subsystem, modes are well separated.

Thus, a classical set-up has been chosen: a flexible rectangular plate backing a parallelepipedic rigid cavity designed with appropriate dimensions and materials. Substituting a small part of the rigid wall by the active device allowed us to evaluate the effects of an impedance change.

The system considered is presented in Figure 6. The rectangular cavity has a volume $V = L_x \times L_y \times L_z$, bounded by walls including flexible, rigid and absorbing parts of respective areas A_p, A_r, A_a. The flexible wall is a simply supported thin plate of thickness h_p. Young's modulus, material density and the Poisson ratio are denoted by E_p, ρ_p and ν_p respectively. The normal acoustic impedance over A_a is Z_a. The plate is excited by an external load $F = F_o e^{j\omega t}$ at the point (x_F, y_F), ω being the angular frequency. (The time dependence term $e^{j\omega t}$ will be omitted in the equations.)

3.1. ANALYTICAL DESCRIPTION

If purely numerical techniques such as finite element methods are the most appropriate for solving vibroacoustic problem, reference cases are helpfully selected through analytical developments. The problem can be solved by using different modal expansion methods. Modal expansion over coupled modes requires the pre-determination of the latter, which is often possible only by finite-element-based techniques. Pope in 1971 [33] suggested to use an expansion over uncoupled *in vacuo* plate modes and cavity modes, fluid–structure interactions being accounted for through modal coupling. The cavity modes satisfy the impedance

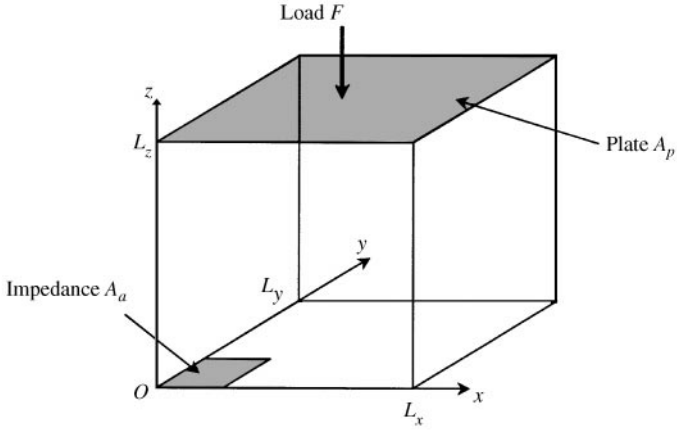

Figure 6. Three-dimensional cavity including an impedance and an elastic plate.

boundary conditions in Pope's formulation [33], and can be usually determined only from numerical techniques. Dowell *et al.* [28] will be followed to include impedance effects through rigid cavity mode coupling. The sudden impedance change at part of the cavity walls makes the use of rigid cavity modes suspect and convergence must be carefully verified in order to be confident in the space where the solution is sought. In practice, modal truncation will be increased until the solution does no more evolve. Remaining discrepancies are observed in the pressure field only in the immediate vicinity of the impedance discontinuities. The uncoupled structural and acoustic fields will be employed and a matrix formalism used to write the coupled equations.

3.1.1. Structural motion equation

The z-normal displacements w of the plate middle surface are governed by the structural motion equation, given in the harmonic analysis by

$$D\nabla^4 w - \rho_p h_p \omega^2 w = p^c - p^e, \tag{3}$$

where D is the plate flexural rigidity,

$$D = \frac{E_p h_p^3}{12(1-\nu^2)}, \tag{4}$$

p^c and p^e are the internal surface pressure due to the cavity and the external load respectively. If the plate is simply supported, the normal *in vacuo* undamped modes are

$$S_M(\mathbf{X}_p) = \sin\left(\frac{p\pi x}{L_x}\right)\sin\left(\frac{q\pi y}{L_y}\right), \tag{5}$$

(p, q) being the modal indices of the Mth mode and $\mathbf{X}_p$ the plate location vector. The corresponding modal angular frequency is

$$\omega_M = \left(\frac{D}{\rho_p h_p}\right)^{1/2}\left[\left(\frac{p\pi}{L_x}\right)^2 + \left(\frac{q\pi}{L_y}\right)^2\right]. \tag{6}$$

The displacement w can be expanded on these modes according to

$$w(\mathbf{X}_p) = \sum_{M=1}^{\infty} W_M S_M(\mathbf{X}_p). \tag{7}$$

The modal expansion is substituted into the dynamics equation (3) and the orthogonality relations between the undamped modes used to show that

$$\rho_p h_p(\omega_M^2 - \omega^2) W_M \int_{A_p} S_M S_M \,\mathrm{d}A = \int_{A_p} p^c S_M \,\mathrm{d}A - \int_{A_p} p^e S_M \,\mathrm{d}A. \tag{8}$$

It follows that

$$(k_M^2 - k^2) W_M = \frac{1}{M_M^p c_0^2} \left[\int_{A_p} p^c S_M \, \mathrm{d}A - \int_{A_p} p^e S_M \, \mathrm{d}A \right], \tag{9}$$

where $k_M = \omega_M / c_0$, $M_M^p = \rho_p h_p \int_{A_p} S_M S_M \, \mathrm{d}A$ is the modal mass. The external load is $p^e = F_0 \delta(x - x_F) \delta(y - y_F)$. This gives

$$(k_M^2 - k^2) W_M = \frac{1}{M_M^p c_0^2} \left[\int_{A_p} p^c S_M \, \mathrm{d}A - F_0 S_M(x_F, y_F) \right], \tag{10}$$

where $M = 1, 2, \ldots, \infty$.

3.1.2. Acoustic subsystem equation

When no source is present in the cavity, the acoustic pressure p satisfies the Helmholtz equation

$$\nabla^2 p + k^2 p = 0 \tag{11}$$

where $k = \omega / c_0$. The boundary conditions are

$$\frac{\partial p}{\partial n} = \rho_0 \omega^2 w \quad \text{on } A_p, \tag{12}$$

$$\frac{\partial p}{\partial n} = -\rho_0 \mathrm{j}\omega \frac{p}{Z_a} \quad \text{on } A_a, \tag{13}$$

$$\frac{\partial p}{\partial n} = 0 \quad \text{on } A_r, \tag{14}$$

n being the positive outward normal component.

The acoustic pressure is also expanded on the normal undamped modes of the rectangular cavity with rigid boundary conditions:

$$p(\mathbf{X}) = \sum_{N=1}^{\infty} P_N \phi_N(\mathbf{X}), \tag{15}$$

$\mathbf{X}$ is the cavity location vector and

$$\phi_N(\mathbf{X}) = \cos\left(\frac{m\pi x}{L_x}\right) \cos\left(\frac{n\pi y}{L_y}\right) \cos\left(\frac{t\pi z}{L_z}\right), \tag{16}$$

(m, n, t) being the modal indices of the Nth mode. The corresponding modal angular frequency is

$$\omega_N = c_0 \left[\left(\frac{m\pi}{L_x}\right)^2 + \left(\frac{n\pi}{L_y}\right)^2 + \left(\frac{t\pi}{L_z}\right)^2 \right]^{1/2}. \tag{17}$$

Applying Green's theorem to Helmholtz equation (11) yields

$$\int_V (\nabla^2 \phi_N - \phi_N \nabla^2 p)\, \mathrm{d}V = \int_A \left(p \frac{\partial \phi_N}{\partial n} - \phi_N \frac{\partial p}{\partial n} \right) \mathrm{d}A, \tag{18}$$

where $A = A_r \cup A_a \cup A_p$.

The modal expansion, together with the undamped acoustic modes orthogonality properties and boundary conditions, allows one to recast equation (18) in the form

$$(k^2 - k_N^2) P_N \int_V \phi_N \phi_N \, \mathrm{d}V = -\rho_0 \omega^2 \int_{A_p} \phi_N w \, \mathrm{d}A + \mathrm{j} \frac{\omega \rho_0}{Z_a} \int_{A_p} \sum_{R=1}^{\infty} \phi_n \phi_R P_R \, \mathrm{d}A \tag{19}$$

for $N = 1, 2, \ldots, \infty$; $k_N = \omega_N / c_0$ is the wavenumber associated with the Nth acoustic mode.

The structural–acoustic coupling is apparent in equations (10) and (19): equation (10) includes a term which describes the load exerted by the internal pressure on the plate dynamics, while equation (19) incorporates the plate displacements as source terms for the acoustic equation. Substituting the modal expansions of p^c and w into equations (10) and (19), respectively, yields the solution to the coupled system.

3.1.3. Matrix resolution of the coupled system

Denoting the acoustic modal mass as $M_N^a = \rho_0 \int_V \phi_N \phi_N \, \mathrm{d}V$, the structural–acoustic coupling term in equation (19) becomes

$$\begin{aligned} \int_{A_p} \phi_N w \, \mathrm{d}A &= \int_{A_p} \phi_N \sum_{M=1}^{\infty} W_M S_M \, \mathrm{d}A \\ &= \sum_{M=1}^{\infty} W_M \int_{A_p} S_M \phi_N \, \mathrm{d}A \\ &= \sum_{M=1}^{\infty} W_M A_p B_{N,M}. \end{aligned} \tag{20}$$

The $B_{N,M}$ term is related to the modal spatial coupling between the Nth cavity mode and the Mth plate mode. $B_{N,M}$ can be analytically determined. For given

(m, n, t) acoustic and (p, q) structural modes, one has

$$B_{N,M} = \begin{cases} (-1)^t \dfrac{pq}{\pi^2} \dfrac{[1-(-1)^{(p-m)}][1-(-1)^{(q-n)}]}{(p^2-m^2)(q^2-n^2)} & \text{if } m \neq p \text{ and } n \neq q, \\ 0 & \text{other cases.} \end{cases} \tag{21}$$

Also a coupling term between the acoustic modes is introduced:

$$C_{N,R} = \frac{1}{A_a} \int_{A_a} \frac{\phi_N \phi_R}{Z_a} \, \mathrm{d}A. \tag{22}$$

Thus, how the value and location of the impedance affects the acoustic field is described via the coupling of the rigid cavity modes. The integral in equation (22) can be analytically determined by using equation (16).

Introducing equations (20), (22) and the acoustic modal mass into equation (19) leads to

$$(k^2 - k_N^2) P_N = -\frac{k^2 \rho_0^2 c_0^2 A_p}{M_M^a} \sum_{M=1}^{\infty} B_{N,M} W_M + \mathrm{j} \frac{k \rho_0^2 c_0 A_a}{M_N^a} \sum_{R=1}^{\infty} C_{N,R} P_R \tag{23}$$

for $N = 1, 2, \ldots, \infty$.

In the same way, using the modal expansion of p^c and introducing $B_{N,M}$ allows equation (10) to be recast in the form

$$(k_M^2 - k^2) W_M = \frac{A_p}{M_M^p c_0^2} \sum_{N=1}^{\infty} B_{N,M} P_N - \frac{F_0}{M_M^p c_0^2} S_M(x_F, y_F) \tag{24}$$

for $M = 1, 2, \ldots, \infty$.

The internal damping which limits the levels at resonances is now introduced in the modelling. Losses are often evaluated via measurements, the modal damping being estimated *in situ* at each resonance of the system. This allows completing the analytical description of the system with additional modal loss factors. Viscous modal loss factors for the cavity and the plate are retained here. We denote them by η_N and η_M respectively. Structural damping (internal friction within the material and at joints between components) is usually considered as hysteretic but viscous damping occurs also when a structure is moving in a fluid (radiation damping). Because of its simplicity, an equivalent viscous damping model usually replaces dampings of all nature. A detailed study of modal loss factors in structural–acoustic systems is given by Cheng and Lesueur [34]. Thus, the modal co-ordinates P_N and W_M of the acoustic pressure and plate displacements satisfy the following system:

$$(k^2 - \mathrm{j}\eta_N k_N k - k_N^2) P_N - \mathrm{j} \frac{k \rho_0^2 c_0 A_a}{M_N^a} \sum_{R=1}^{\infty} C_{N,R} P_R + \frac{k^2 \rho_0^2 c_0^2 A_p}{M_M^a} \sum_{M=1}^{\infty} B_{N,M} W_M = 0,$$

$$\frac{A_p}{M_M^p c_0^2} \sum_{N=1}^{\infty} B_{N,M} P_N + (k^2 - \mathrm{j}\eta_M k_M k - k_M^2) W_M = \frac{F_0}{M_M^p c_0^2} S_M(x_F, y_F). \tag{25}$$

The system is solved via a matrix formulation developed in the same way as in Hong and Kim [30]. Recall that a high modal truncation is required when Z_a departs far from the rigid wall case [35], in order to account for the acoustic modes used which satisfy the rigid boundary condition.

The acoustic and displacements fields are deduced from the modal vectors P_N and W_M. It is also straightforward to evaluate the time-averaged acoustic potential energy by using orthogonality properties:

$$E_{pot} = \frac{1}{4\rho_0 c_0^2} \int_V |p(\mathbf{X})|^2 \, \mathrm{d}V = \frac{1}{4\rho_0 c_0^2} \sum_{N=1}^{\infty} M_N^a |P_N|^2. \tag{26}$$

Again, this expression defines the global sound pressure index, which allows one to quantify the reduction produced by an impedance change.

3.2. EXPERIMENTAL SET-UP

3.2.1. Subsystem achievement

The rectangular cavity used in the experiments is built from high density, impervious fibreboard covered by a thin film of reflecting paint, in order to provide the best approximate of the assumed acoustically hard behaviour of the walls. The cavity dimensions are $L_x = 0{\cdot}9$ m, $L_y = 1{\cdot}1$ m and $L_z = 1$ m, avoiding strong overlaps between acoustic modes within the frequency bandwidth studied (below 400 Hz). The same criterion has been retained in designing the flexible wall, a plate of dimensions $0{\cdot}9 \text{ m} \times 1{\cdot}1 \text{ m} \times 0{\cdot}006$ m, made from 2017A aluminium presenting the following characteristics $E_p = 7{\cdot}4 \times 10^{11}$ Pa, $\rho_p = 2850$ kg/m^3 and $v_p = 0{\cdot}3$. Modal acoustic and structural densities are roughly equivalent in the frequency range. Particular attention has been paid to the practical achievement of simply supported boundary conditions. Translational displacements are blocked while rotations about the cavity edges supporting the plate are allowed. A method of practical realization inspired by Ochs and Snowdon [36] has been used: a 0·3 mm thick steel strip is glued in part under the plate along its perimeter, while the other part is clamped on the cavity edges, as shown in Figure 7. This technique allows one to achieve hinged boundary conditions in remarkable agreement with those expected from the theory. As can be seen in Table 1, only a weak stiffness is introduced by the steel strip. Furthermore, acoustic leaks between the plate and the cavity are avoided.

3.2.2. The actuator

An electrodynamic shaker (Bruël & Kjaer 4810) is hung from a rigid support in order to avoid static load, and is related to the plate via a fine rod. In the analytical description, it is assumed that the external load does not depend on the vibroacoustic response of the system. An impedance head (Bruël & Kjaer 8001) placed between the shaker and the rod allows one to measure the input load, and eventually to proceed so that it remains constant (equal to 1 N) during all the

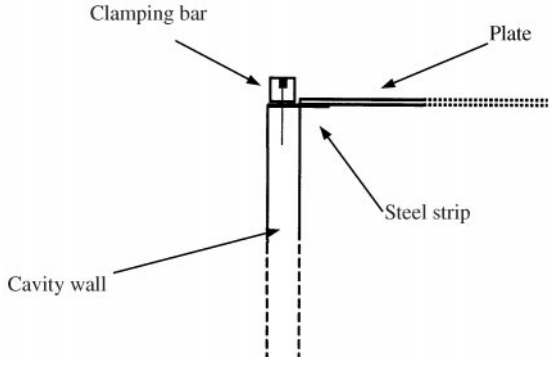

Figure 7. Realization of the simply supported boundary condition.

TABLE 1

Primary cavity and plate modal frequencies

Number	Cavity modes			Plate modes		
N or M	(m, n, t)	f_N^{th} (Hz)	$f_N^{\exp}$ (Hz)	(p, q)	f_M^{th} (Hz)	$f_M^{\exp}$ (Hz)
1	(0, 0, 0)	0	—	(1, 1)	30	29
2	(0, 1, 0)	156	150	(1, 2)	66	67
3	(0, 0, 1)	171	168	(2, 1)	84	84
4	(1, 0, 0)	190	187	(2, 2)	120	120
5	(0, 1, 1)	231	238	(1, 3)	126	128
6	(1, 1, 0)	246	248	(3, 1)	173	173
7	(1, 0, 1)	256	255	(2, 3)	180	179
8	(1, 1, 1)	300	302	(3, 2)	209	206
9	(0, 2, 0)	312	312	(1, 4)	210	212
10	(0, 0, 2)	343	343	2, 4)	264	257
11	(0, 2, 1)	356	358	(3, 3)	270	265
12	(1, 2, 0)	365	365	(4, 1)	299	296
13	(0, 1, 2)	377	377	(1, 5)	318	319
14	(2, 0, 0)	381	381	(4, 2)	335	336
15	(1, 0, 2)	392	393	(3, 4)	354	361

experiment. The plate is excited at the location $x_F = 0{\cdot}36$ m, $y_F = 0{\cdot}46$ m, which does not correspond to any vibration node for all significant modes.

3.2.3. The acoustic impedance control

The controlled impedance is at first that presented by the $0{\cdot}12\text{ m} \times 0{\cdot}12$ m square flat membrane of a loudspeaker, driven via the direct control method and digital signal processing as described before. Real impedance values are relatively easily achieved. Next, the hybrid impedance method, which uses a feedback scheme, is implemented and an absorbing surface of equivalent area to that of the first method is obtained.

3.2.4. The measurement set-up

An important aim of the study is to give an insight into the evolution of the acoustic and structural fields induced by the actual active impedance when practically implemented. The variation of the acoustic potential energy relative to the rigid wall case defines the first index, as in the one-dimensional case. The kinetic energy is the indicator retained for the plate displacement field. Its calculation from the plate modal co-ordinates is similar to that of the acoustic potential energy. The plate modal co-ordinates will be presented relative to the uncontrolled (rigid impedance) case.

The experimental magnitudes of the first modes are obtained from the processing of acceleration measurements at 21 randomly distributed locations over the plate. The technique, reported by Fuller *et al.* [37], uses the theoretical mode shapes of the simply supported plate and a modal space projection of *in situ* vibration measurements.

The global sound level variation is evaluated with an antenna of 16 microphones regularly spaced along the x-axis inside the cavity. The automatic translation along the y- and z-axis allows a refined scanning of the acoustic field throughout the cavity. Seventeen locations are chosen along the y-axis, 10 along the z-axis, yielding 2720 measurement points and a cost function *representative* of the acoustic potential energy,

$$J_p = \sum_{i=1}^{N_m} \overline{p(x_i)^2} \quad \text{where } N_m = 2720. \tag{27}$$

Note that $\overline{p(x_i)^2}$ in equation (27) refers to a time measurement and includes contributions that are not correlated with the excitation (background noise or contributions due to non-linear effects for instance).

3.2.5. System identification procedure

A validation step is necessary to evaluate the agreement between the theoretical and actual modal characteristics. Furthermore, the fitting between them yields the modal damping coefficients.

Theoretical and experimental resonance frequencies of each uncoupled subsystem are reported in Table 1. Acoustic modes are determined from frequency response functions between an internal acoustic source and a microphone, while the plate is blocked. Similarly, the experimental evaluation of the plate modes requires its decoupling from the acoustic cavity, which is filled with fibreglass. The modes are deduced from frequency response functions between the impedance head of an impact hammer and a fixed accelerometer. The obtained experimental resonance frequencies are in good agreement with those of the theoretical rigid cavity and *in vacuo* plate: a few Hertz maximum error is revealed by the analysis. A good agreement is also found between theoretical and experimental mode shapes of the subsystems. As an illustration, Figure 8 presents the measured and theoretical shapes of the (3, 1) plate mode and those of the (1, 1, 0)-cavity mode, plate vibration measurements being performed over 144 evenly distributed locations.

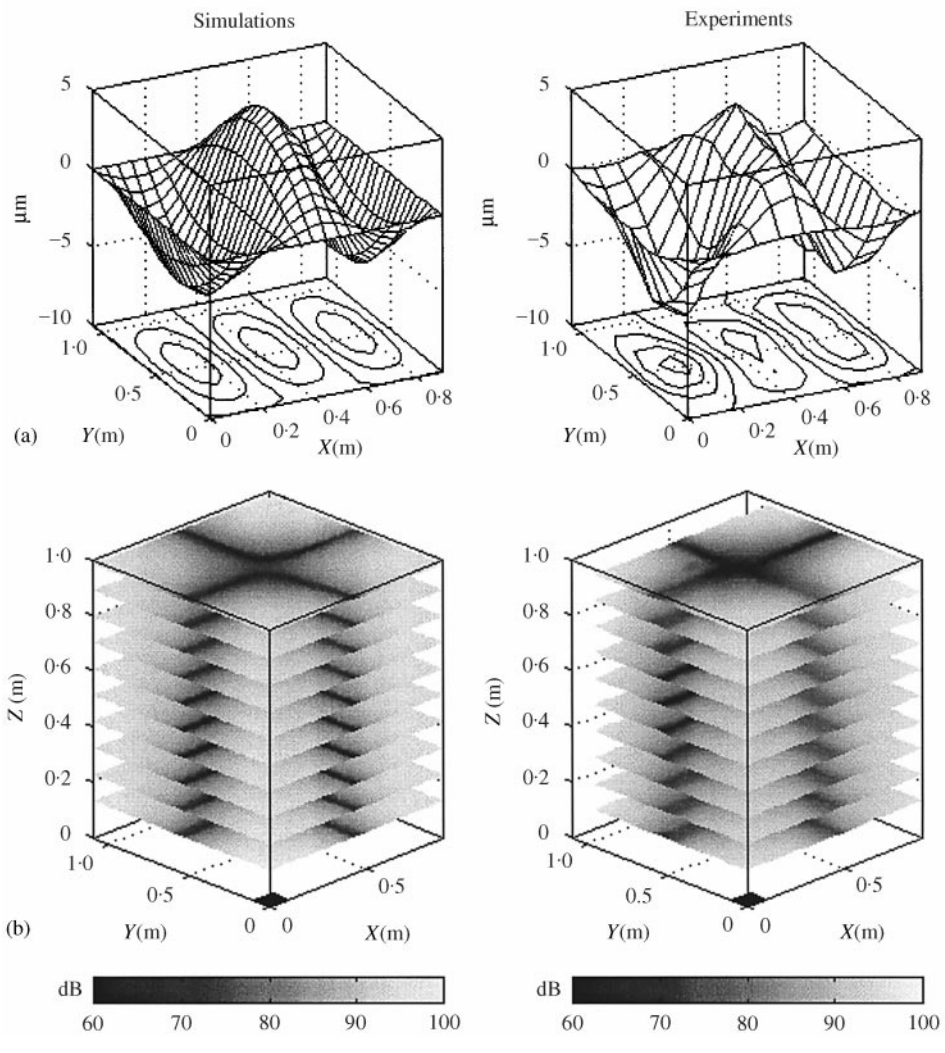

Figure 8. Example of theoretical and experimental modal shapes for the cavity–plate system: (a) simply supported plate mode (3, 1); (b) rigid cavity mode (1, 1, 0).

It may be noted that, during the experiments, modal loss factors were also identified for each subsystem considered independently. The method consists in measuring the transient response of one system after switching off the source. Modal loss factors are deduced from decay values at some resonance frequencies. The mean value $\eta_N = 3 \times 10^{-3}$ is retained for each mode of the cavity, and in the same way, $\eta_M = 6 \times 10^{-3}$ is obtained for all plate resonances.

3.3. RESULTS AND COMMENTS FOR HARMONIC EXCITATIONS

The set-up will be first experimented for three typical cases involving an excitation at one single frequency and inducing fundamentally different coupling

behaviours. For each case, different impedance values are successively assigned, the rigid wall case being used again as reference to quantify the acoustic potential energy variation: $\Delta E_p(\zeta) = E_p(\zeta) - E_p(\infty)$ in the calculations and $\Delta J_p(\zeta) = J_p(\zeta) - J_p(\infty)$ in the experiments, where J refers to the measured estimate of the energy E, given by equation (27).

The direct control method is employed to assign the impedances $Z = 0$ (a null pressure), $Z = Z_0/2$, Z_0, $2Z_0$ and $4Z_0$. It may also be noted that the Z_0 impedance, which is the total absorbent impedance when implemented at the terminal cross-section of a plane waveguide, corresponds no longer to the maximum acoustic energy that can be absorbed. Finally, the hybrid impedance is also tested for each excitation case via a *feedforward control*, the control method being chosen in order to evaluate the hybrid system performances when used in optimum conditions.

3.3.1. Choice of three fundamental frequency excitations

For the harmonic excitation case, particular frequencies are chosen with regard to the structural–acoustic coupling presented by the whole system. Two classes of coincidence, say frequency and spatial coincidences [38], exist between cavity and plate modes. The former corresponds to a spectral proximity between an acoustic and a plate resonance: in this case, an excitation at a frequency near these resonances induces high levels in both subsystems. The latter accounts for the spatial coupling between the cavity and the plate. This effect, which is analytically governed by the $B_{N,M}$ coefficient, for two specific acoustic and structural modes, does not depend on the respective natural frequencies: it may appear between two frequency-distant modes, and is rather a *measure of spatial match between plate and cavity modes* [39]. Table 2 presents the possible modal pairs for the spatial coupling. A very important selectivity is observed with a large coupling coefficient for very few modes only. This coupling coefficient may be seen as the flow rate through the plate resulting from the pressure and displacement fields induced by two mode shapes, thereby explaining the null coupling coefficient which is obtained for an antisymmetrical product, as graphically represented in Figure 9.

TABLE 2

Selectivity of panel–cavity modal spatial coupling: $\surd \Leftrightarrow B_{N,M} \neq 0$ (*o*, *odd number*; *e*, *even number*; *n*, *arbitrary number*). *From Pan and Bies* [39]

Panel modes	Cavity modes			
	(o, o, n)	(e, e, n)	(o, e, n)	(e, o, n)
(o, o)		$\surd$		
(e, e)	$\surd$			
(o, e)				$\surd$
(e, o)			$\surd$	

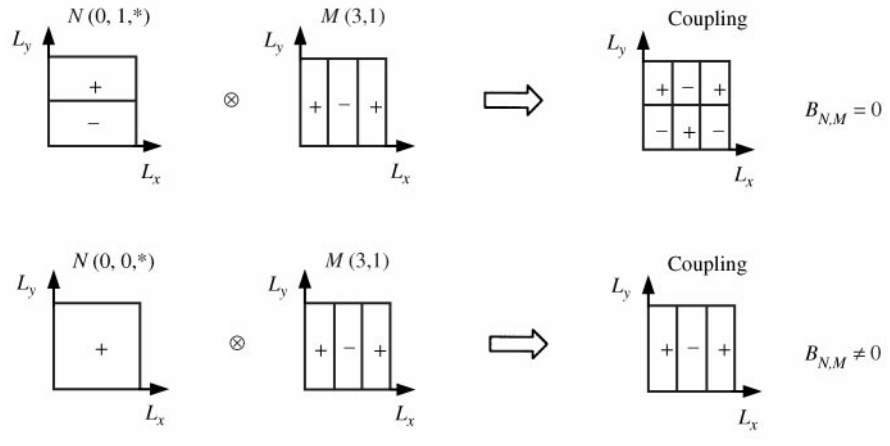

Figure 9. $B_{N,M}$ coefficients resulting from the coupling between the Nth cavity mode and the Mth plate mode.

Three typical harmonic excitation cases have been selected from preliminary test [40]. Theoretical and experimental studies are not carried out at exactly the same frequency because of the weak differences in modal characteristics, which persist between those theoretically expected and actually experimented. Thus, the excitation frequencies are weakly shifted in order to reproduce similar spatial-frequency behaviours.

In the first case, the excitation frequency ($\approx$249 Hz) is close to the natural frequency of the (1, 1, 0)-cavity tangential mode. The system response is dominated by the cavity, and the mode is referred to as *cavity-controlled* [39]. The x, y-tangential waves induce a weak fluid–structure coupling: no frequency coincidence occurs, only a weak spatial coupling appears in the low-frequency range with the (2, 2) and (2, 4) plate modes.

In the second case, the excitation frequency ($\approx$173 Hz) is close to the natural frequencies of both (0, 0, 1) cavity axial mode and (3, 1) plate mode. The system response is said to be dominated by a plate–cavity mode. Moreover, acoustic z-axis waves induce a uniform pressure distribution on the plate, which provides a significant fluid–structure spatial coupling with the (3, 1) plate mode (this is also alternatively shown by the relatively important value taken by the associated $B_{N,M}$ coefficient). Many experiments are required to exhibit this strong structural–acoustic spatial coupling, and it must be emphasized that this spatial and frequency coincidence is unique in the low-frequency range.

The third case chosen corresponds to an off-resonance frequency. The excitation frequency ($\approx$265 Hz) lies between the (1, 0, 1) and (1, 1, 1) cavity mode natural frequencies, on the one hand, and between the (2, 4) and (3, 3) structural modes, on the other. Neither an important frequency nor spatial coincidence occurs in this case. Since it has been experimented in the case of the one-dimensional cavity that an impedance change may increase the total acoustic potential energy in a significant manner, the off-resonance behaviour will be also examined before attempting noise reductions for broadband excitations.

3.3.2. Validation procedure for the system response

As explained above and confirmed by a preliminary study, a high modal truncation is required by the formulation, especially when the controlled impedance departs from the rigid case. Practically, the number of modes retained in the summation results from a compromise between the computer ability and the desired accuracy. In sum, calculations including 300 cavity modes (up to 1300 Hz) and 75 plate modes (up to 1600 Hz) provide a good agreement with experiments for the frequency range of interest (below 400 Hz).

Figure 10 may be considered as the last validation. The sound pressure field obtained from simulation and experiments is represented over specific planes for the three predefined excitation frequencies in the most demanding case of soft impedance. A very good agreement is observed except for the off-resonance excitation. The latter case involves low levels and is more sensitive to inaccuracies.

3.3.3. Impedance control at a frequency associated with a weak acoustic–structural coupling

The weak coupling case is shown in Figure 11. The very good agreement confirms the significant global noise reductions, which may be achieved in the cavity with a soft impedance. Indeed, an 8 dB attenuation is measured, an important value if one compares the active impedance area to the total area of the walls: approximately 0·25% is treated. At this cavity resonance, the null impedance produces a frequency shifting of the acoustic modal characteristics thereby inducing a less important primary acoustic energy supply. It is worth noting the large reductions also achieved by active impedances adjusted to Z_0 via the hybrid impedance design. Scanning the sound pressure variations throughout the cavity reveals that attenuation may be termed as *global* and not localized in the vicinity of the active impedance.

The variations of the plate displacement modal co-ordinates are reported for different impedance values in Figures 12 and 13. Slight discrepancies between experimental and numerical results in observed. The plate response is dominated by several modes and we note that an impedance change does not induce important displacement variations. Investigating the relative modal phases (not reported here) also shows that no modal rearrangement occurs for any impedance case.

We conclude noting that these investigations extend previous one-dimensional results [27]. If no significant coupling appears between the primary source and the enclosed sound field, a pressure release implies significant global noise reductions in the cavity, when excited near an acoustic resonance frequency.

3.3.4. Impedance control at a frequency associated with a strong acoustic–structural coupling

The evolution of the potential energy as a function of the reduced impedance is shown in Figure 14. The curve shapes are similar, although the modelling exhibits sharper variations. The greatest sound reduction is still obtained with the null impedance, although to a weaker extent than that of the weak coupling experiment presented above. The best global reduction experimentally achieved is of 2 dB.

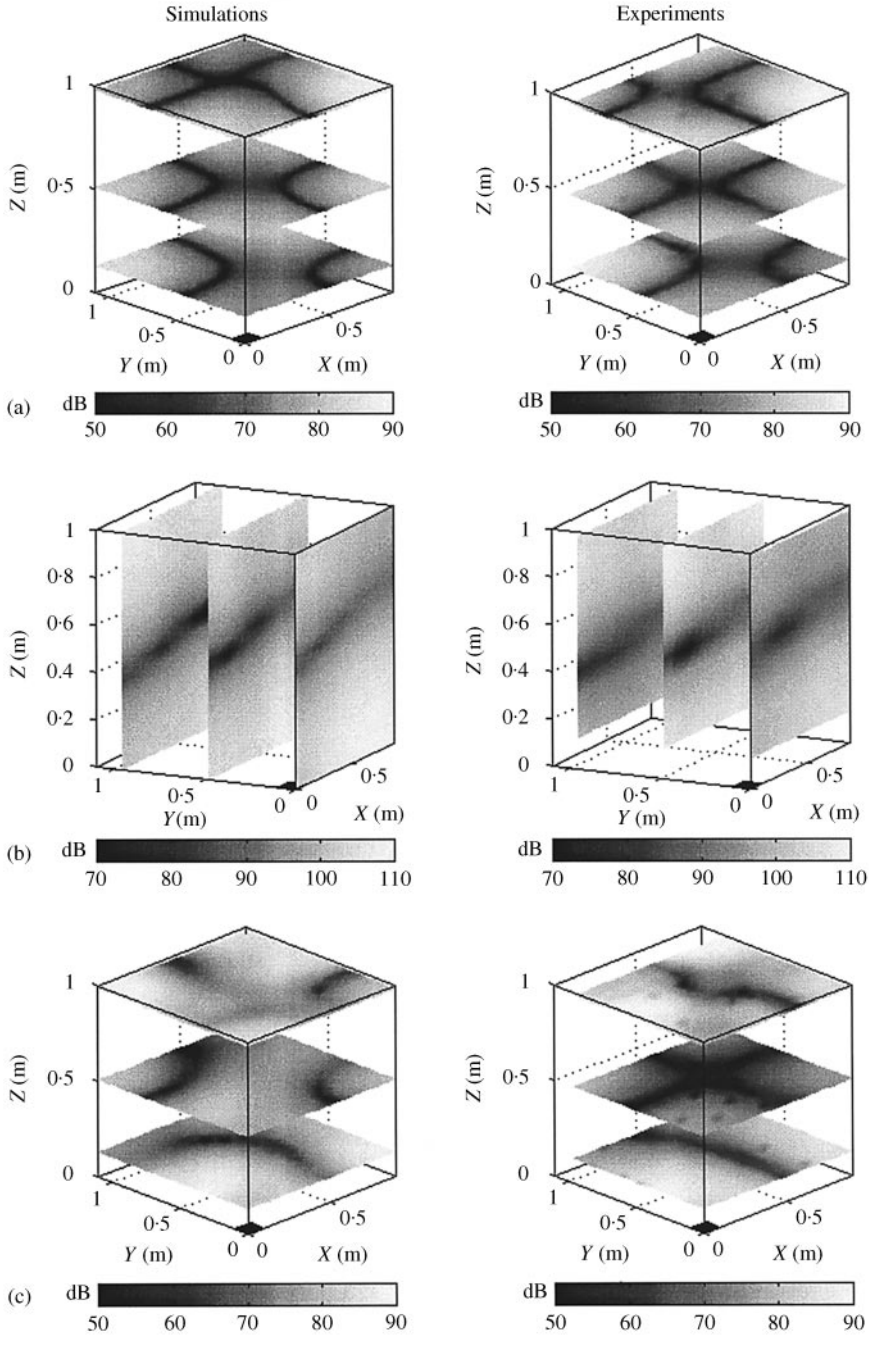

Figure 10. Theoretical and experimental sound pressure level evolution for the three considered cases with a soft impedance ($\zeta = 0$) at the origin: (a) weak coupling acoustic resonance, (b) strong coupling acoustic resonance, (c) off-acoustic resonance.

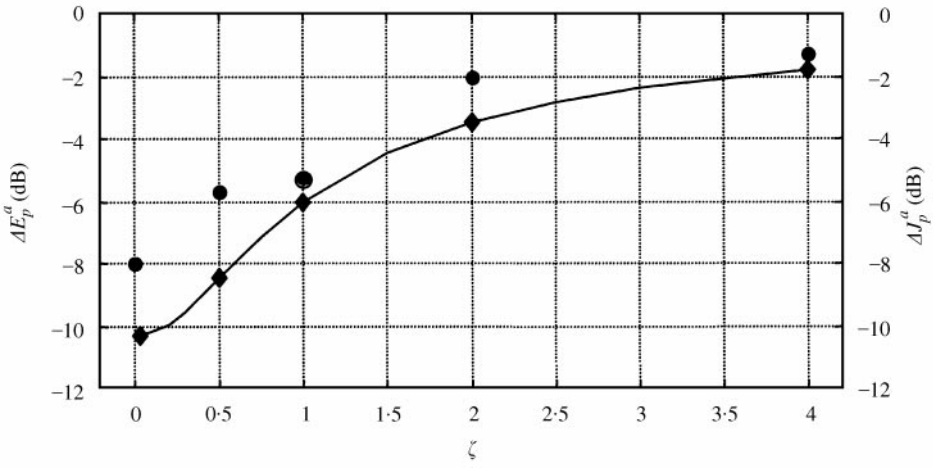

Figure 11. Acoustic potential energy variation versus reduced impedance on weak coupling resonance case: ◆, simulations; ●, experiments; ○, porous layer.

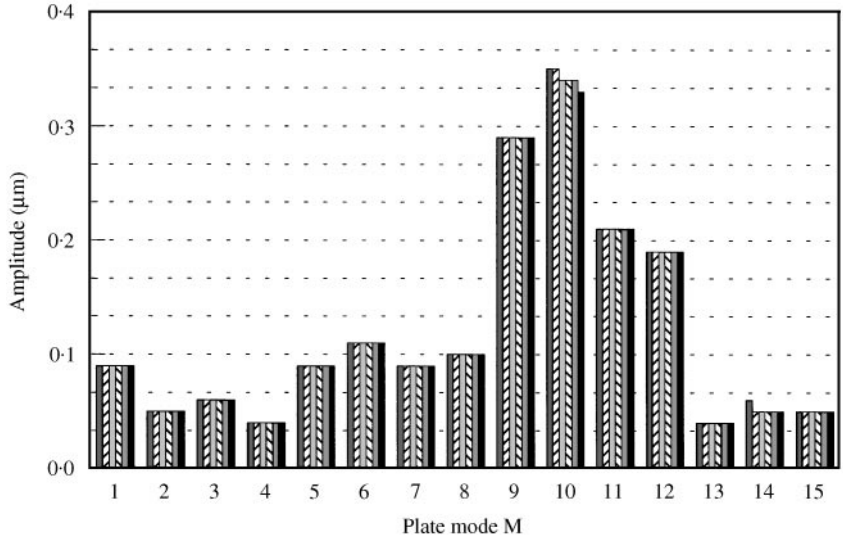

Figure 12. Theoretical plate modal displacements versus reduced impedance on weak coupling resonance excitation: ■, $\zeta = 0$; ▨, $\zeta = 0{\cdot}5$; ■, $\zeta = 1$; ▧, $\zeta = 2$; ■, $\zeta = 4$; ■, ζ_∞.

This behaviour is explained by the variation of the plate modal displacements as a function of the impedance (see Figures 15 and 16 for the calculated values and measurements). As expected, the plate response is dominated by the unique (3, 1)-plate mode and a fairly good agreement at any impedance value is noted. In comparison with other impedances, $\zeta = 0$ yields a significant vibration increase for the (3, 1)-plate mode. Contrary to what was observed in the weak coupling case, the null impedance produces a vibration increase, which significantly limits the sound reduction in the cavity. It is interesting to note, however, that when the reduced

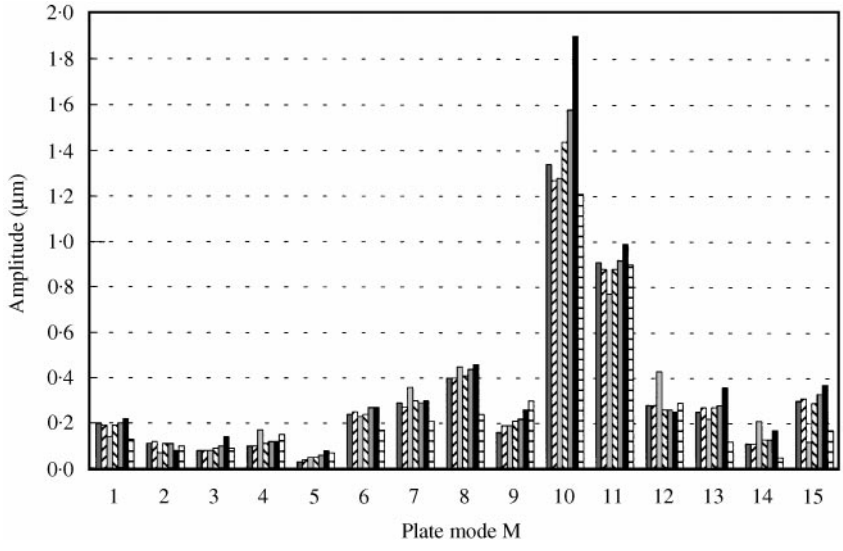

Figure 13. Experimental plate modal displacements versus reduced impedance on weak coupling resonance excitation: ■, $\zeta = 0$; ▨, $\zeta = 0{\cdot}5$; ▩, $\zeta = 1$; ▧, $\zeta = 2$; ▩, $\zeta = 4$; ■, ζ_∞; ▤, ζ_{porous}.

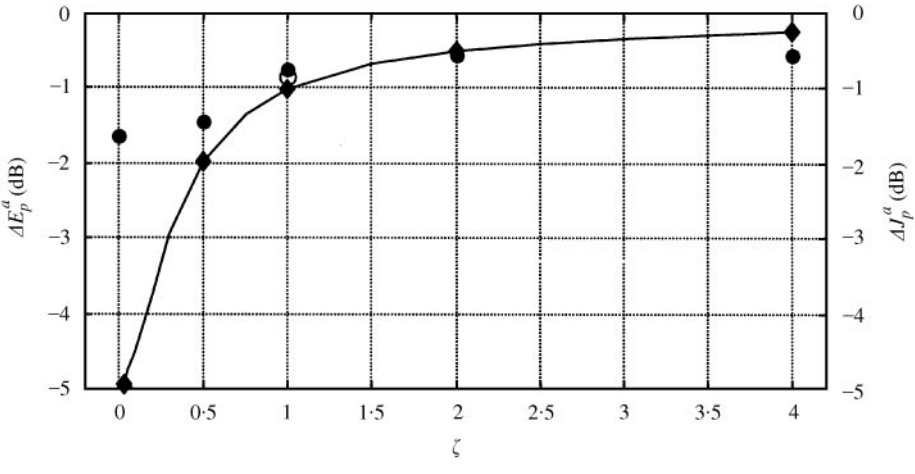

Figure 14. Acoustic potential energy variation versus reduced impedance on strong coupling resonance case: ◆, simulations; ●, experiments; ○, porous layer.

impedance is close to unity, the vibration increase is limited, on the one hand, while sound reductions are close to those obtained in the soft impedance case, on the other. No change of the plate modal relative phase occurs in all experiments, and the acoustic attenuation is global in the cavity.

This cavity–plate coupling case exhibits a behaviour, which is very sensitive to active impedance: global reductions are obtained at the expense of an important increase in plate displacements, usually referred to as "modal regeneration".

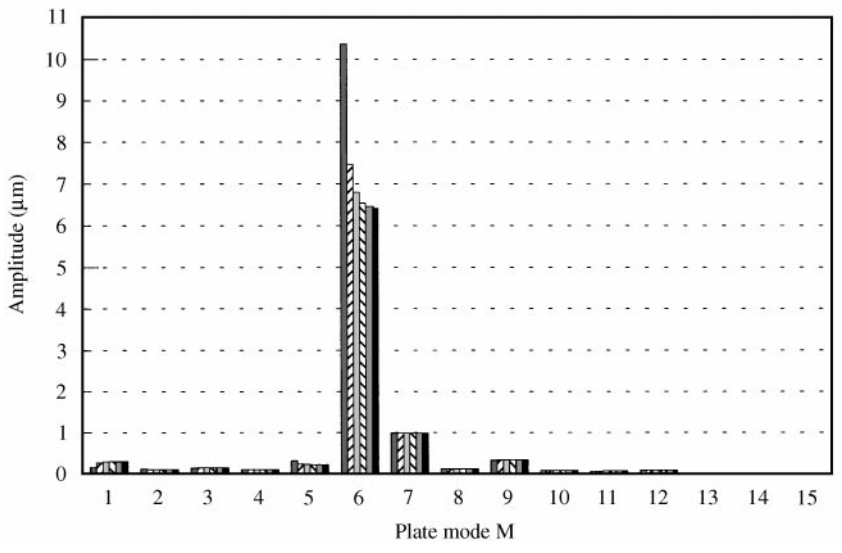

Figure 15. Theoretical plate modal displacements versus reduced impedance on strong coupling resonance excitation: ■, $\zeta = 0$; ▨, $\zeta = 0{\cdot}5$; ■, $\zeta = 1$; ▨, $\zeta = 2$; ■, $\zeta = 4$; ■, ζ_∞.

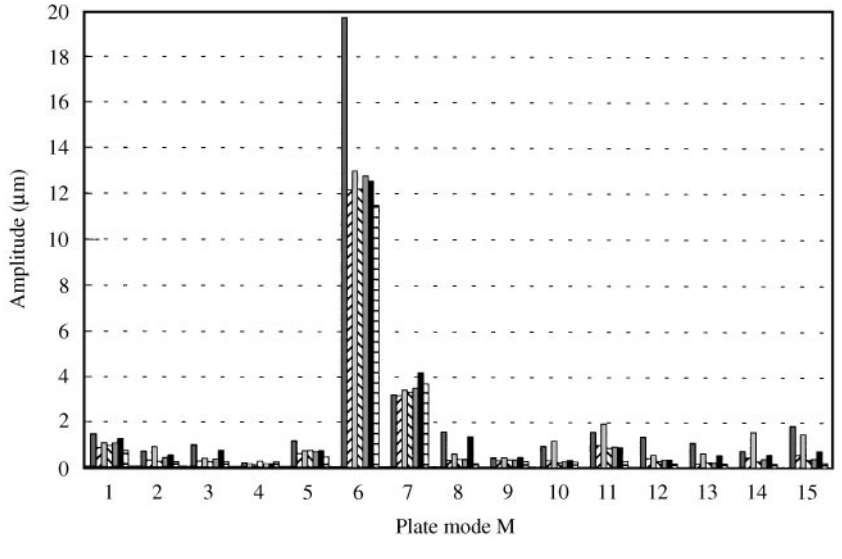

Figure 16. Experimental plate modal displacements versus reduced impedance on strong coupling resonance excitation: ■, $\zeta = 0$; ▨, $\zeta = 0{\cdot}5$; ■, $\zeta = 1$; ▨, $\zeta = 2$; ■, $\zeta = 4$; ■, ζ_∞; ▤, ζ_{porous}.

3.3.5. Impedance control at an off-resonance frequency

The evolution of the acoustic potential energy as a function of the impedance is reported in Figure 17. A global pressure increase is induced by the soft impedance with a measured maximum variation of 5 dB. This effect is similar to that observed in the uncoupled one-dimensional cavity [27]: acoustic resonances are shifted by

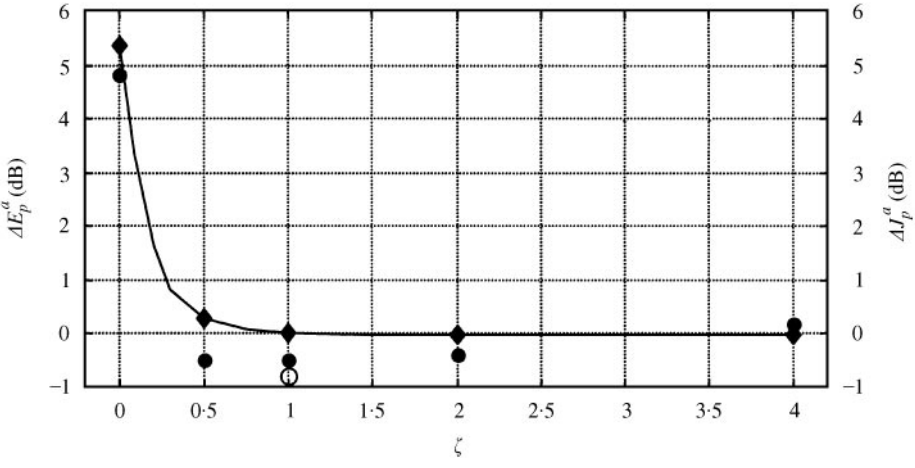

Figure 17. Acoustic potential energy variation versus reduced impedance on off-resonance case: ◆, simulations; ●, experiments; ○, porous layer.

a soft impedance, thus inducing an important sound level increase at an initially off-resonance frequency. Higher impedance values do not induce any increase in the acoustic energy; weak reductions are even experimentally measured, particularly in the case of the hybrid impedance.

The modal magnitudes of the plate displacements as a function of the reduced impedance are shown in Figures 18 and 19. Neither the amplitude nor the modal relative phase is affected by the different impedance values. These results also extend those obtained with the one-dimensional cavity, when excited at an anti-resonant frequency.

3.4. RESULTS AND COMMENTS FOR BROADBAND EXCITATIONS

Investigating means to tackle the widest class of acoustic problems implies accounting for broadband noise. In this context, a null impedance, which appears to be the most efficient for reducing noise levels at resonant frequencies, may create new resonances if the control is not selective and hence becomes less attractive. In the first part of this paper, the effectiveness of an absorbing termination in controlling broadband one-dimensional fields has been pointed out. These observations hold for the three-dimensional case also presented in this paper: the Z_0 impedance yields global acoustic reduction at cavity resonances while avoiding off-resonance regeneration effects. Moreover, no significant plate displacement variation is observed during all the experiments.

Accordingly, new tests are carried out with a view to determine the effectiveness of the hybrid feedback control in reducing three-dimensional fields in the plate–cavity system. Several broadband excitations were considered. We present thereafter the results obtained for the 200–400 and 150–350 Hz frequency ranges; the resonance frequencies of 11 cavity modes and 10 plate modes for the former,

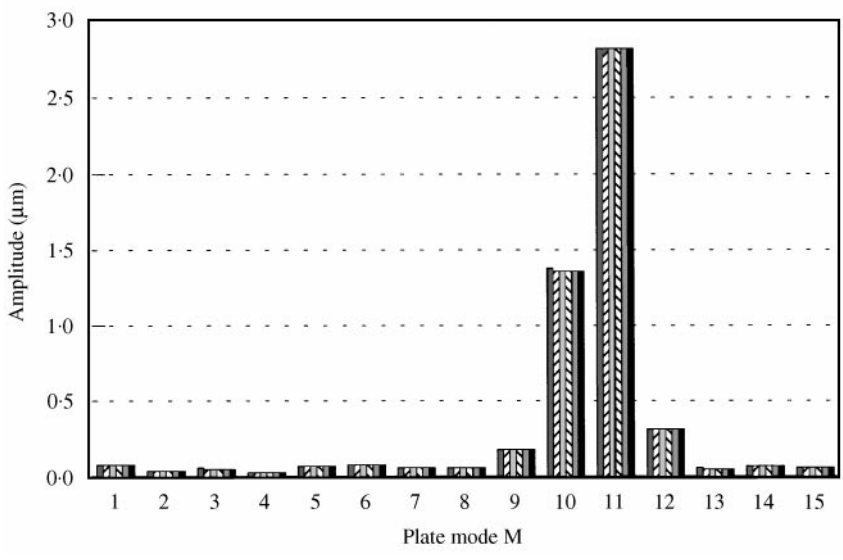

Figure 18. Theoretical plate modal displacements versus reduced impedance on off-resonance excitation: ■, $\zeta = 0$; ▨, $\zeta = 0{\cdot}5$; ▩, $\zeta = 1$; ▧, $\zeta = 2$; ▩, $\zeta = 4$; ■, ζ_∞.

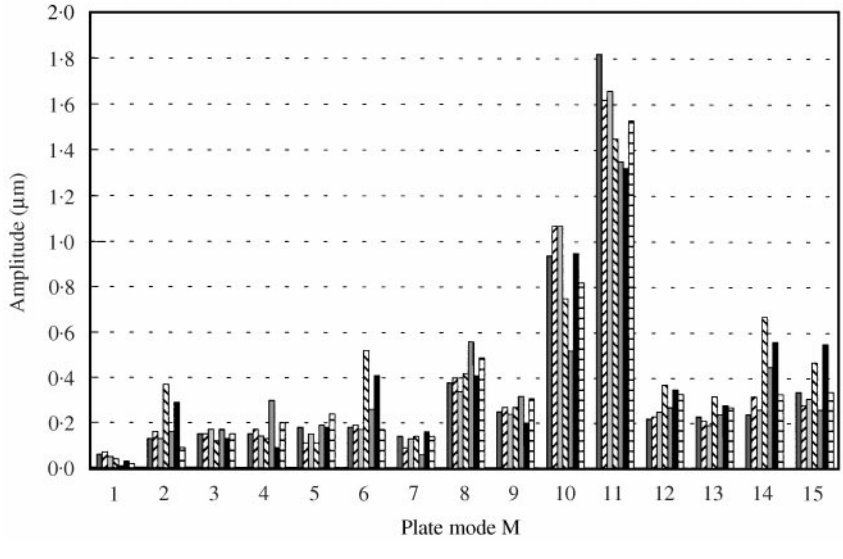

Figure 19. Experimental plate modal displacements versus reduced impedance on off-resonance excitation. ■, $\zeta = 0$; ▨, $\zeta = 0{\cdot}5$; ▩, $\zeta = 1$; ▧, $\zeta = 2$; ▩, $\zeta = 4$; ■, ζ_∞; ▤, ζ_{porous}.

and the resonance frequencies of 9 modes of both subsystems for the latter are involved. The numerical simulations are conducted with a frequency step of 0·25 Hz and the acoustic potential energy for a specific impedance is evaluated according to

$$E_p^a(\zeta) \propto \int_{f_{\min}}^{f_{\max}} E_p^a(\zeta, f)\, \mathrm{d}f.$$

The control filter achieves an active pressure release of 10–20 dB at the rear face of the porous layer.

The $0{\cdot}12\text{ m} \times 0{\cdot}12\text{ m}$ area impedance used in a first attempt did not allow significant reductions in the experiments, despite encouraging simulations. Among other factors, the global acoustic measurement provided by the microphones may be invoked: a Fourier analysis downstream of each antenna microphone was too cumbersome to be considered, and uncontrolled frequency ranges may prevent the correct energy evaluation. The too small absorbing area and the control effectiveness may be also invoked. To cope in part with these problems, an increase of the active impedance effect is intended by increasing its effective area via the collection of four active elementary cells, each including an independent feedback control. This set-up proved its effectiveness during previous experiments in an anechoic room [1]. The hybrid impedance area is extended to $0{\cdot}28\text{ m} \times 0{\cdot}28\text{ m}$, approximately 1% of the total surface bounding the cavity. Although simulations still remain more attractive than measurements, significant global noise reductions clearly come out for the two broadband excitations considered. $\Delta J_p\,[200\text{–}400\text{ Hz}] = 2{\cdot}3\text{ dB}$ and $\Delta J_p\,[150\text{–}350\text{ Hz}] = 3{\cdot}7\text{ dB}$ are obtained in the experiments while $\Delta E_p\,[200\text{–}400\text{ Hz}] = 5{\cdot}0\text{ dB}$ and $\Delta E_p\,[150\text{–}350\text{ Hz}] = 9{\cdot}6\text{ dB}$ were expected from the simulation. Experiments and simulations reveal no evident plate vibration increase induced by the active impedance. The experiments conducted with a relatively reduced controlled area, generally confirm the interest of the feedback hybrid method in globally silencing enclosed sound fields.

It may be added that other impedances were not considered for controlling the acoustic field induced by the broadband excitations. The reason why $z = 0$ has been ruled out stems from the calculated frequency variation of the acoustic potential energy shown in Figures 20 and 21 (impedance area: $0{\cdot}12\text{ m} \times 0{\cdot}12\text{ m}$). As in the one-dimensional case, the effect of a null impedance is to slightly shift the cavity resonances to upper frequencies while keeping the strong resonant behaviour of the enclosed sound field. Thus, no global sound pressure level reduction may be expected with a soft impedance for the broadband excitations considered. Alternatively, impedance reduced values closer to that of air ($0{\cdot}5 \leqslant \zeta \leqslant 2$) provide an additional damping on each acoustic mode, leading to a decrease in the potential energy for the whole frequency range. An important work devoted to the optimization of the hybrid control and its location (see the work by Martin and Bodrero [41] for that purpose) remains. As an example, a considerable additional sound level reduction could be obtained with a different dispatching of the same treated area, as shown in Figure 22. The acoustic potential energy calculated for a [150–350 Hz] broadband excitation is 5 dB lower for almost all impedances, when the absorbing surface is distributed at each corner of the cavity bottom.

4. CONCLUSION

Experiments devoted to the control of enclosed sound fields via active changes in wall impedance have been presented in this paper. Particular attention has been

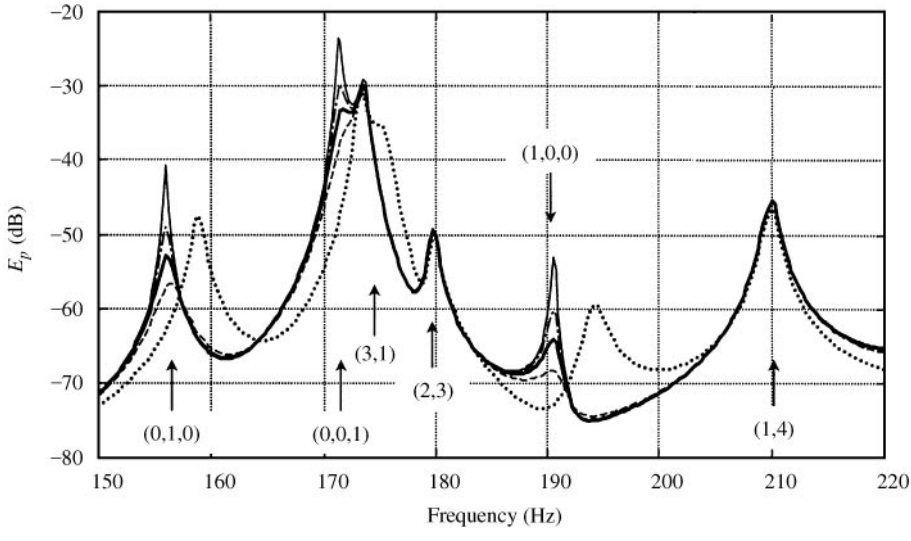

Figure 20. Acoustic potential energy evolution versus frequency as a function of different reduced impedance values. An array with 2 indices refers to the corresponding plate mode, an array with 3 indices refers to the corresponding cavity mode: · · · · · · ·, $\zeta = 0$; – – –, $\zeta = 0{\cdot}5$; —, $\zeta = 1$; – · – · –, $\zeta = 2$; —, ζ_∞. $(*, *)$ → plate; $(*, *, *)$ → cavity.

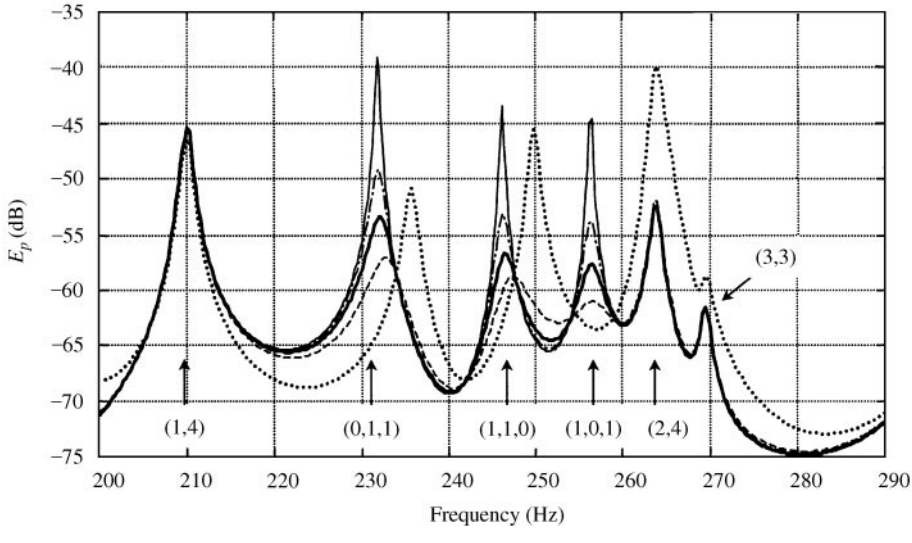

Figure 21. Acoustic potential energy evolution versus frequency as a function of different reduced impedance values. An array with 2 indices refers to the corresponding plate mode, an array with 3 indices refers to the corresponding cavity mode: · · · · · ·, $\zeta = 0$; – – –, $\zeta = 0{\cdot}5$; —, $\zeta = 1$; – · – · –, $\zeta = 2$; —, ζ_∞. $(*, *)$ → plate; $(*, *, *)$ → cavity.

focused on the reduction provided by an impedance when its value is close to that of air, an objective readily achieved practically by hybrid passive/active feedback control. The interest of the method presented lies in actively silencing cavities when feedforward control cannot be applied, and the overall physical context dictates the

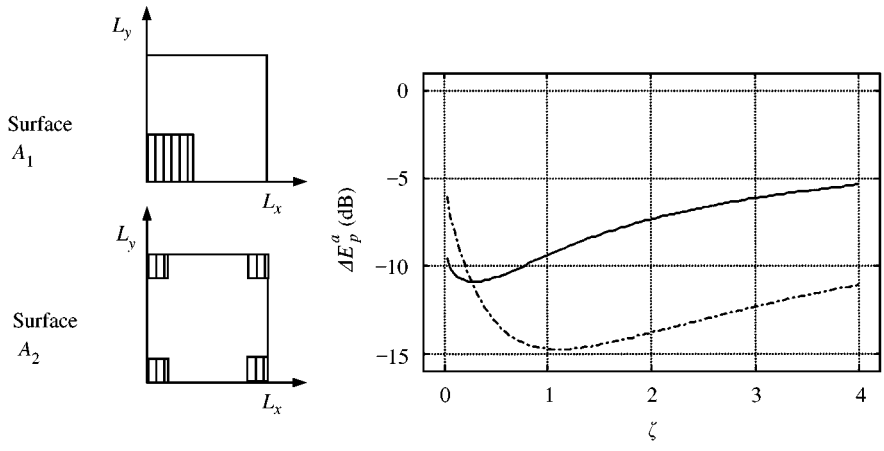

Figure 22. Acoustic potential energy variation versus reduced impedance for two distributions of the treated surface: [150–350 Hz]: ——, A_1; – · – · –, A_2.

control to be designed on a feedback scheme. One-dimensional fields have been successfully controlled for a broadband excitation, by using a hybrid feedback control method. Then, the direct control of impedance has been implemented in a cavity where three-dimensional fields propagate, allowing to review the mechanisms, which dictate noise reductions for different acoustic–structural couplings. The attenuation level has been seen to depend on the interactions between the acoustic and structural systems. At a cavity resonance involving a weak coupling, an impedance value close to that of air (Z_0) induces useful attenuations, although less important than those created by a soft impedance (a pressure release). At a cavity resonance involving a strong coupling, the Z_0 impedance allows again sound level reduction. For an off-resonance excitation, the soft impedance implies important sound level *increases* while the Z_0 impedance still allows reductions. Further experiments conducted for two broadband excitations including several plate and cavity resonance frequencies showed that the hybrid device allows significant sound pressure level reductions without significant structure vibration increase. In each case considered, reductions are obtained even when an impedance of relatively small area is used. The results reported are very promising although the trends seen have to be confirmed by working with other frequencies.

Current research is also directed towards the improvement of the hybrid control itself (integration, control selectivity, robustness). Combining passive and active methods is a pragmatic approach using a simplified control system. It proves to be particularly relevant when more conventional active or passive methods are not suited. Many elements must be also taken into account in order to enhance methods such as the development of multiple-point feedback control techniques and the optimization of impedance value and location. A general process concerning practical implementation of impedance control has to be defined.

ACKNOWLEDGMENTS

Part of this work has been conducted while D. Thenail was post-doctoral fellow of the Centre national d'Etudes Spatiales. Organizers and participants of the Pôle Vibroacoustique are gratefully acknowledged.

REFERENCES

1. M. Furstoss, D. Thenail and M. A. Galland 1997 *Journal of Sound and Vibration* **203**, 219–236. Surface impedance control for sound absorption: direct and hybrid passive/active strategies.
2. P. Lueg 1936 *US Patent* 2043416. Process of silencing sound oscillations.
3. P. A. Nelson and S. J. Elliott 1992 *Active Control of Sound*. London: Academic Press.
4. C. R. Fuller and J. D. Jones 1987 *Journal of Sound and Vibration* **112**, 389–395. Experiments on reduction of propeller induced interior noise by active control of cylinder vibration.
5. A. R. D. Curtis, P. A. Nelson, S. J. Elliott and A. J. Bullmore 1987 *Journal of the Acoustical Society of America* **81**, 624–631. Active suppression of acoustic resonance.
6. A. R. D. Curtis, P. A. Nelson and S. J. Elliott 1990 *Journal of the Acoustical Society of America* **88**, 2265–2268. Active reduction of a one-dimensional enclosed sound field: an experimental investigation of three control strategies.
7. R. L. Clark and D. G. Cole 1995 *Journal of the Acoustical Society of America* **97**, 1710–1716. Active damping of enclosed sound fields through direct rate feedback control.
8. R. L. Clark, K. D. Frampton and D. G. Cole 1996 *Journal of Sound and Vibration* **195**, 701–718. Phase compensation for feedback control of enclosed sound fields.
9. C. Deffayet and P. A. Nelson 1988 *Journal of the Acoustical Society of America* **84**, 2192–2199. Active control of low-frequency harmonic sound radiated by a finite panel.
10. C. R. Fuller 1990 *Journal of Sound and Vibration* **136**, 1–15. Active control of sound transmission/radiation from elastic plates by vibration inputs: I. Analysis.
11. D. R. Thomas, P. A. Nelson and S. J. Elliott 1990 *Journal of Sound and Vibration* **139**, 351–355. Experiments on the active control of the transmission of sound through a clamped rectangular plate.
12. S. D. Snyder and C. H. Hansen 1991 *Journal of Sound and Vibration* **170**, 519–525. Mechanisms of active noise control by vibration sources.
13. V. L. Metcalf, C. R. Fuller, R. J. Sylcox and D. E. Brown 1992 *Journal of Sound and Vibration* **153**, 387–402. Active control of sound transmission/radiation from elastic plates by vibration inputs: II. Experiments.
14. J. Pan, S. D. Snyder, C. H. Hansen and C. R. Fuller 1992 *Journal of the Acoustical Society of America* **91**, 2056–2066. Active control of far-field sound radiated by a rectangular panel: a general analysis.
15. R. L. Clark and C. R. Fuller 1992 *Journal of the Acoustical Society of America* **91**, 3321–3329. Modal sensing of efficient acoustic radiators with polyvinylidene fluoride distributed sensors in active structural acoustic control approaches.
16. C. R. Fuller, S. J. Elliott and P. A. Nelson 1996 *Active Control of Vibration*. London: Academic Press.
17. D. Guicking and E. Lorentz 1984 *ASME Journal of Vibration Acoustics, Stress Reliability and Design* **106**, 393–396. Active impedance control for one-dimensional sound.
18. D. Guicking and K. Karcher 1984 *ASME Journal of Vibration Acoustics, Stress Reliability and Design* **106**, 389–392. Active sound absorber with porous plate.
19. D. Guicking, K. Karcher and M. Rollwage 1985 *Journal of the Acoustical Society of America* **78**, 1426–1434. Coherent active methods for applications in room acoustics.

20. G. C. Nicholson and P. Darlington 1991 *Proceedings of the Institute of Acoustics* **13**, 155–164. Smart surfaces for building acoustics.
21. D. Thenail and M. A. Galland 1992 *Proceedings Idee-Force EUR'ACOUSTICS*, *W4*, *Ecole Centrale de Lyon*, *France*. Development of an active anechoical boundary.
22. F. Orduña-Bustamante and P. A. Nelson 1992 *Journal of the Acoustical Society of America* **91**, 2740–2747. An adaptive controller for the active absorption of sound.
23. D. Thenail, M. A. Galland, M. Furstoss and M. Sunyach 1994 *Proceedings of the ASME Winter Annual Meeting*, *Chicago*, *IL*, *DE*-75, *AM*-16*D*, 441–448. Absorption by an actively enhanced material.
24. S. Benyene and R. A. Burdisso 1997 *Journal of the Acoustical Society of America* **101**, 1512–1515. A new hybrid passive/active noise absorption system.
25. C. A. Gentry, C. Guigou and C.R. Fuller 1997 *Journal of the Acoustical Society of America* **101**, 1771–1778. Smart foam for applications in passive–active noise radiation control.
26. H. F. Olson and E. G. May 1953 *Journal of the Acoustical Society of America* **25**, 1130–1136. Electronic sound absorber.
27. D. Thenail, O. Lacour, M. A. Galland and M. Furstoss 1997 *Acustica United with Acta Acustica* **83**, 1039–1044. The active control of wall impedance.
28. E. H. Dowell, G. F. Gorman III and D. A. Smith 1977 *Journal of Sound and Vibration* **52**, 519–542. Acoustoelasticity: general theory, acoustic modes and forced response to sinusoidal excitation, including comparisons with experiment.
29. J. Pan, C. H. Hansen and D. A. Bies 1990 *Journal of the Acoustical Society of America* **87**, 2098–2108. Active control of noise transmission through a panel into a cavity. I: analytical study.
30. K. L. Hong and J. Kim 1995 *Journal of Sound and Vibration* **188**, 561–600. Analysis of free vibration of structural–acoustic coupled systems, Part I: development and verification of the procedure, Part II: two- and three-dimensional examples.
31. C. Carme 1988 *Acustica* **66**, 233–246. Absorption acoustique active dans les cavités auditives.
32. P. A. Nelson, J. K. Hammond, P. Joseph and S. J. Elliott 1990 *Journal of the Acoustical Society of America* **87**, 963–975. Active control of stationary random sound fields.
33. L. D. Pope 1971 *Journal of the Acoustical Society of America* **50**, 1004–1018. On the transmission of sound through finite closed shell: statistical energy analysis, modal coupling, and non-resonant transmission.
34. L. Chen and C. Lesueur 1989 *Journal d'Acoustique* **2**, 105–118. Influence des amortissemenets sur la réponse vibroacoustique: étude théorique d'une plaque excitée acoustiquement et couplée à une cavité.
35. L. P. Franzoni and E. H. Dowell 1995 *Journal of the Acoustical Society of America* **97**, 687–690. On the accuracy of modal analysis in reverberant acoustical systems with damping.
36. J. B. Ochs and J. C. Snowdon 1975 *Journal of the Acoustical Society of America* **58**, 832–840. Transmissibility across simply supported thin plates. I. Rectangular and square plates with and without damping layers.
37. C. R. Fuller, C. H. Hansen and S. D. Snyder 1991 *Journal of Sound and Vibration* **145**, 195–215. Active control of sound radiation from a vibrating rectangular panel by sound sources and vibration inputs: an experimental comparison.
38. C. Lesueur 1988 *Rayonnement acoustique des structures. Vibroacoustique, interaction fluid-structure*. Paris: Eyrolles.
39. J. Pan and D. A. Bies 1990 *Journal of the Acoustical Society of America* **87**, 691–707. The effect of fluid-structural coupling on sound waves in an enclosure—theoretical part.

40. O. LACOUR, D. THENAIL and M. A. GALLAND 1997 *Proceedings of ASME DETC'97*, 16*th Biennial Conference on Mechanical Vibration and Noise*, *Sacramento*, *CA*, *VIB*-3795. Actively silencing a cavity by acoustic impedance changes.
41. V. MARTIN and A. BODRERO 1997 *Journal of Sound and Vibration* **204**, 331–357. An introduction to the control of sound fields by optimising impedance locations on the wall of an acoustic cavity.

.